Phase stability, mechanical, electronic, magnetic and thermodynamic properties of the Pd_2PrX(X=Cl, F) compounds: An Ab-initio study

S. Benatmane[a,b,*], M. Affane[a], Y. Bouali[c], B. Bouadjemi[a], S. Cherid[a] and W. Benstaali[a]

[a] *Faculté des Sciences et techniques, Département des sciences et techniques, Université Abdelhamid Ibn Badis de Mostaganem, 27000, Mostaganem, Algérie.*
[*] *e-mail: saadia.benotmane@univ-mosta.dz*
[b] *Laboratoire de Modélisation et Simulation en Sciences des Matériaux, Université Djillali Liabès de Sidi Bel-Abbès, Sidi Bel-Abbès, 22000, Algérie.*
[c] *Power equipment Characterization and Diagnosis Laboratory, University of Science and Technology Houari Boumediene, Algiers, Algeria.*

Received 27 March 2022; accepted 21 June 2022

Many of the known examples of half-metallic ferromagnets HMF are oxides, sulfides, or Heusler alloys have attracted some interest for their potential use in spintronics. In order to achieve such understanding we have performed an ab-initio calculations with spin polarization using plane-wave pseudo potential technique based on the density-functional theory (DFT), the exchange-correlation potential was treated with the generalized gradient approximation (PBE-GGA), whereas for the treatment of on-site electron-electron correlations the PBE-GGA+U approximation (where U is the Hubbard Coulomb energy term) are applied for the calculation of the structural, electronic, elastic and magnetic properties of Pd_2PrX (X=Cl, F). The results showed that for Pd_2PrCl and Pd_2PrF, Hg_2CuTi-type structure is energetically more stable than Cu_2MnAl-type structure at the equilibrium volume. Electronically, Pd_2PrCl and Pd_2PrF exhibit half-metallicity with small band gaps of 0.06 and 0.25 eV respectively with GGA-PBE+U in the spin-down channels whereas spin-up channels are conducting. The calculated total magnetic moment of 2.00 μB per formula unit is very close to integer value and agree well with the Slater-Pauling rules ($M_{\text{tot}} = 34 - Z_{\text{tot}}$), where the magnetic moment is basically carried by Pr atoms. However, the elastic properties show that Pd_2PrX (X=Cl, F) compounds are ductile and anisotropic according to the analysis of B/G and Cauchy's pressure. The Thermodynamic properties were also analyzed using the quasi-harmonic Debye model. Both the compounds are found structurally stable.

Keywords: DFT; electronic properties; structural properties; full-heusler; half-metallicity; elastic properties; thermodynamic properties.

DOI: https://doi.org/10.31349/RevMexFis.69.011003

1. Introduction

During the last two decades, due to their possible applications in spintronics/magnetoelectronics, for half-metallic ferromagnetic compounds with unique electronic structures, one of the two spin channels is semiconducting and the other is metallic. As promising spintronic candidates, they exhibit a complete spin polarization of carriers near the Fermi level (EF) [1, 2] Heusler alloys are named for the German mining engineer and chemist Friedrich Heusler, who investigated Cu-Mn-Al alloys around the year 1900. Heusler compounds are ternary intermetallic compounds, which have been known since 1903 [3].

Heusler alloys are represented by two variants: the half-Heusler XYZ compounds and the full-Heusler X_2YZ alloys. The stoichiometric composition of the Full-Heusler is X_2YZ, where X and Y represent two different transition metals (or a rare earth metal (RE)), and Z represents a p element of the 3rd, 4th, or 5th main group. Full-Heusler compounds are found in either Cu_2AlMn-type or Hg_2CuTi-type, as shown in Fig. 1.

Computer simulation is the process of mathematical modelling, performed on a computer, which is designed to predict the behaviour of or the outcome of a real-world or physical system. Since they allow to check the reliability of chosen mathematical models, computer simulations have become a useful tool for the mathematical modeling of many natural systems in physics (computational physics), astrophysics, climatology, chemistry, biology and manufacturing [4–8].

Although the family of Heusler phases contains a huge number of representatives, there is still a wide potential for inventive materials with principally interesting properties. Up to now, most Heusler alloys have been synthesized experimentally or predicted theoretically by means of density functional calculations contain transition metals 3d, however, there are few reports on the new type of Heusler compounds with rare earth elements [9–15].

To date, there are no experimentally and theoretically investigations on the Heusler alloys containing chlorine Cl or fluorine F Motivated by this, we have employed first-principles calculations founded on density functional theory and quasi-harmonic Debye model in which the phononic effects are contemplated to explore the high-pressure and high-temperature physical properties of the new Heusler alloys: Pd_2PrCl and Pd_2PrF with Hg_2CuTi-type structure, appropriate consideration is assigned to the predictions of the structural, elastic, magnetic, electronic properties and the pressure-volume-temperature relationship, bulk modulus,

heat capacity, Debye temperature, and Entropy of the Pd_2PrX for the first time and we found they are HM materials and useable in spintronics processes.

2. Method of calculations

The first principles calculations were performed by employing FP-LAPW approach [16], based on the DFT [17] as implemented in WIEN2K code [18]. The Kohn Sham equations are solved self consistently using FP-LAPW method, and quasi-harmonic Debye model in which the phononic effects are considered based on GIBBS code [19] have been used to investigate thermodynamic properties of full-Heusler alloy Pd2PrX in the pressure and temperature ranges of 0-20 GPa and 0-1000 K, respectively. Employing this model, recently a several of thermodynamic properties of a vast number of Heusler alloys, like as Ni_2ScAl, Ni_2TiAl, Ni_2Val, Co_2CrGe, Mn_2RuGe, Co_2VAl, Co_2VGa, Fe_2ScP, Fe_2ScAs, Hf_2VAl etc., have been performancefully predicted [20–25].

Exchange and correlation effects are treated with a generalized gradient approximation (GGA) given by Perdew *et al.* [26], the Pr 4f electrons are treated using a GGA+U (U=1.08eV) method for the exchange-correlation effect [27].

In the calculations reported here, we use a parameter $R_{MT} * K_{\max} = 9$, which determines matrix size (convergence), where $K_{\max}$ is the plane wave cut-off and R_{MT} is the smallest of all atomic sphere radii. The cutoff energy, which defines the separation of valence and core states, was chosen as -7.0 Ry, for Brillouin zone integrations, a mesh of $14 \times 14 \times 14$ k-points was employed to perform the above calculations, the energy convergence criterion is set to be 1×10^{-6} eV/atom for the total energy calculations, the convergence tolerances were selected as the difference in total energy and the maximum force being within 10^{-5} eV and 10^{-2} eV/Å, respectively. The valence electron configurations of Pd, Pr, F and Cl atoms in the compositions are considered as $4d^{10}$, $4f^3 6s^2$, $2s^2 2p^5$ and $3s^2 3p^5$ respectively, The values of the muffin-tin sphere radius (MTS) for Pd, Pr, Cl and F were adopted to be 2.14, 1.87, 2.05 and 1.92 a.u, respectively.

The valence wave functions inside the spheres are expanded up to $l_{\max} = 10$ while the charge density was Fourier expanded up to $G_{\max} = 24$ and the force convergence criterion is of 0.1 mRy/a.u. The Monkhorst-Pack special k-points were performed using 3000 special k-points in the Brillouin zone [28].

3. Results and discussion

3.1. Structural properties

The full Heusler compounds crystallize in an ordered cubic structure with four interpenetrating face-centered-cubic (FCC) sublattices, which can be defined by four Wyckoff coordinates: A(0,0,0), B(0.25,0.25,0.25), C(0.5,0.5,0.5) and D(0.75,0.75,0.75). Two types of structure with different atomic ordering are present: the Cu_2MnAl structure (Fm3m space group, No. 225), also called $L2_1$- type, in which two X atoms occupy the A and B sites while the Y atom enters into the C site, or the Hg_2CuTi structure (F43m space group, No. 216), also called as XA-type, in which two X atoms occupy the A and C sites while the Y atom enters into the B site. The main group Z atom is always located at the D site for both types. According to the site preference rule in Heusler alloys, the two X atoms with more valence electrons occupy A and C positions and form the $L2_1$-type structure, and the two X atoms with less valence electron occupy A and B positions and form the XA-type structure. The two crystal structures of Pd_2PrX(X=Cl, F) are shown in Fig. 1. For L21-type structure of our compounds, the four Wyckoff sites A, B, C and D are occupied by Pd(A), Pr, Pd(C) and X(Cl, F) atoms, respec-

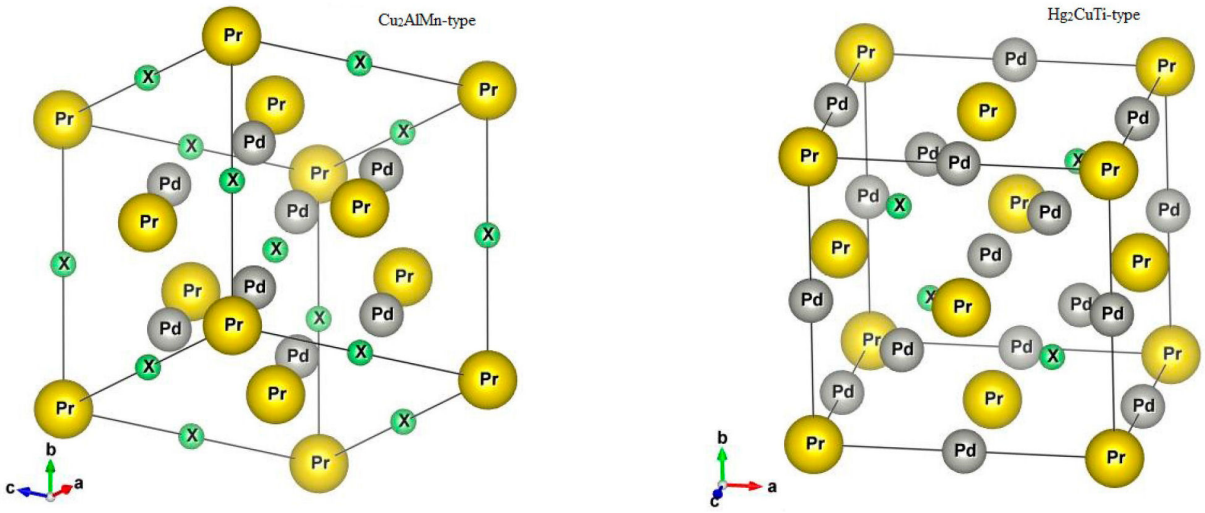

FIGURE 1. Crystal structure of Pd_2PrX (X=Cl,F) Heusler alloy: Cu_2AlMn-type and Hg_2CuTi-type.

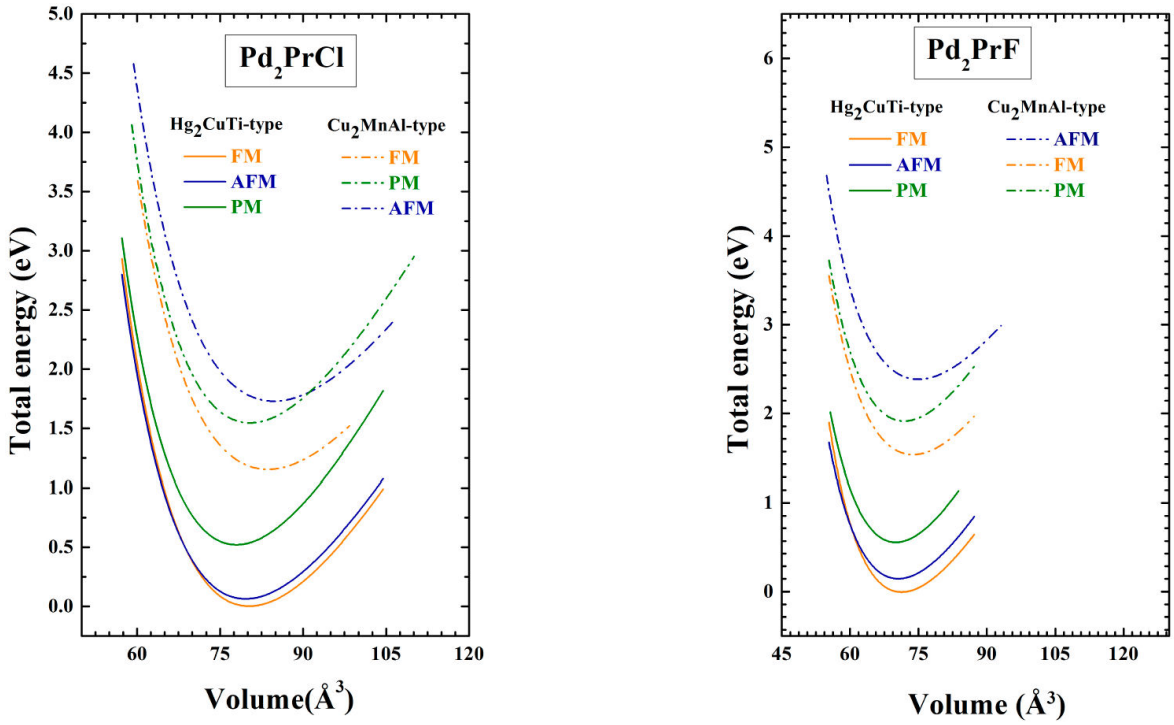

FIGURE 2. Total energies as functions of volume per formula unit are compared for the ferromagnetic (FM), anti-ferromagnetic (AFM) and non-magnetic (NM) states of Pd_2PrX (X=Cl, F) in the Cu_2MnAl and Hg_2CuTi-type structures, using the GGA-PBE approximation.

TABLE I. The calculated equilibrium lattice parameter (a), bulk modulus (B), derivative of bulk modulus (B'), the cohesive energy E_c (eV), formation energy E_f (eV) and the energy difference $E = E_{AFM} - E_{FM}$ (eV) for Pd_2PrCl and Pd_2PrF for the ferromagnetic (FM), anti-ferromagnetic (AFM) and non-magnetic (NM) states for Cu_2MnAl and Hg_2CuTi-type structures by the GGA-PBE and GGA-PBE+U.

Compound	structure		Methods		a(Å)	B(GPa)	B'	E_c(Ry)	E_f(Ry)	ΔE(mEv)
Pd_2PrCl	Hg_2CuTi	Our work	GGA-PBE	FM	6.82	74.23	4.94	-1.15	-0.32	82.49
				NM	6.76	83.24	4.96	-1.11	-0.29	
				AFM	5.40	72.99	5.13	-1.15	-0.32	
			GGA+U	FM	6.85	71.57	4.95	-1.10	-0.29	
	Cu_2MnAl	Our work	GGA-PBE	FM	6.92	65.49	4.74	-1.06	-0.24	
				NM	6.83	78.77	5.08	-1.04	-0.22	
				AFM	5.51	60.96	5.15	-1.02	-0.20	
Pd_2PrF	Hg_2CuTi	Our work	GGA-PBE	FM	6.57	93.69	5.40	-1.27	-0.50	
				NM	6.53	101.13	5.22	-1.23	-0.46	
				AFM	5.20	90.17	5.14	-1.26	-0.49	169.33
			GGA+U	FM	6.58	90.94	5.43	-1.21	-0.45	
	Cu_2MnAl	Our work	GGA-PBE	FM	6.64	78.94	4.41	-1.15	-0.39	
				NM	6.58	92.58	5.14	-1.13	-0.36	
				AFM	5.30	71.20	5.13	-1.09	-0.33	

tively. On the other hand, for the XA-type structure, the four Wyckoff sites A, B, C and D are occupied by Pd(A), Pd(B), Pr and X(Cl, F) atoms, respectively.

In order to find the equilibrium bulk structure of Pd_2PrX (X=Cl and F) compounds, the total energy with respect to the unit cell volume is minimized and fitted to the empirical Murnaghan equation of state [29]. The Energy-Volume curves for the two compounds in the ferromagnetic (FM), anti-ferromagnetic (AFM) and non-magnetic (NM) states for Cu_2MnAl and Hg_2CuTi-type structures were plotted in Fig. 2. Accordingly, in the two compounds, the Hg_2CuTi -type structure in FM state is more stable than other struc-

ture and is introduced as the ground state structure. The equilibrium structural parameters including lattice parameter (a), bulk modulus (B), derivative of bulk modulus (B′), the cohesive energy E_c(eV), formation energy E_f (eV) and the total energy differences between AFM and FM states $E = E_{AFM} - E_{FM}$ for the two compounds for Cu_2MnAl and Hg_2CuTi-type structures in the ferromagnetic (FM), antiferromagnetic (AFM) and non-magnetic (NM) states were listed in Table I.

The cohesive energy (E_c) is always determined as the difference between the average energy of the atoms of a solid (particularly a crystal) and that of the free atoms for Pd_2PrX (X=Cl, F), the E_c is calculated as:

$$E_c^{Pd2PrX} = E_{\text{tot}}^{Pd2PrX} - (2E_{Pd} + E_{Pr} + E_X), \qquad (1)$$

where E_{tot}^{Pd2PrX} is the equilibrium total energy of Pd_2PrX compound, and E_{Pd}, E_{Pr}, and E_X (X=Cl, F) are the total energies of the isolated atoms, the energy of an isolated atom is calculated by using a FCC lattice with lattice parameter of 20 a.u.

The negative values of E_c for Pd_2PrX (X=Cl, F) compounds show that our compounds are expected to be more stable with Cu_2MnAl structure in FM state. So, they are possible to be synthesized in the experiment.

There is no experimental or theoretical data to compare the obtained results.

E_{Pd2PrX}^{form} represents the formation energy of the solid and this one illustrates the energy difference between a crystal and its constituents in bulk structure, which is calculated as:

$$E_{Pd2PrX}^{\text{form}} = E_{\text{tot}}^{Pd2PrX} - (2E_{Pd}^{\text{bulk}} + E_{Pr}^{\text{bulk}} + E_X^{\text{bulk}}) \qquad (2)$$

where E_{tot}^{Pd2PrX} is the equilibrium total energy of Pd_2PrX (X=Cl, F) compounds, E_{Pd}^{bulk}, E_{Pr}^{bulk} and E_X^{bulk} are the total energies of atomic components in bulk structure. The bulk states that adopted in our calculation of Pd is face centered cubic (f.c.c) structure, Pr is hexagonal structure, F is cubic (c) and F is orthorhombic structure. According to Table I, the negative values of formation energies indicate that these two alloys are probable to form and also are thermodynamically stable.

3.2. Elastic properties

Elastic properties of a solid are very essential seeing that they report to diverse principal solid-state characteristics such as equation of state, phonon spectra and interatomic potentials. Elastic properties are also related thermodynamically to the specific heat, thermal expansion, Debye temperature, Gruneisen parameter and melting point. So, it is necessary to determine elastic constants of solids.

Since the structure of our compounds is cubic, which need only three elastic constants in the tensor C_{ij}, which are C_{11} to measure the longitudinal deformation, C_{12} to measure the transversal expansion and the Shear modulus C_{44}, these constants have a primordial influence to find all the major details about the elastic, structural and mechanical properties. As shown in Table II, the values of the calculated C_{ij} constants are positive and $C_{12} < B < C_{11}$, both the compounds satisfy the Born-Huang stability criteria [30–32] as given in the Eq. (3).

TABLE II. The calculated values of the three elastic constants C_{11}, C_{12}, C_{44} (GPa), Kleinman parameter ζ the Cauchy pressure C_P (GPa), the anisotropy factor A, Poisson's ratio ν, Lamé constants λ and μ, Young's modulus E (GPa), the Voigt shear modulus G_V (GPa), the Reuss shear modulus G_R (GPa), the shear modulus G_H (GPa) and Pugh's ratio B/G for Pd_2PrX (X=Cl ,F) by the GGA-PBE and GGA-PBE+U.

	Pd_2PrCl		Pd_2PrF	
	GGA	GGA+U	GGA	GGA+U
C_{11}	128.92	133.72	168.15	132.08
C_{12}	46.89	40.50	56.47	70 37
C_{44}	16.31	20.86	25.12	28.33
B	74.23	71.57	93.69	90.94
ζ	0.505	0.45	0.44	0.65
A	0.39	0.44	0.57	0.91
C_p	30.58	19.64	31.35	42.04
ν	0.35	0.32	0.33	0.35
E	109.25	117.72	148.13	134.11
λ	95.59	79.27	108.10	115.89
μ	40.46	44.59	55.68	49.67
G_V	26.19	31.16	37.40	29.34
G_R	21.48	26.77	32.20	29.28
G_H	23.83	28.96	34.8	29.31
B/G	3.11	2.47	2.69	3.10

$$C_{11} - C_{12} > 0, C_{11} + 2C_{12} > 0. \qquad (3)$$

The bulk modulus B and the shear modulus G are two reputed modules for measuring compressibility and stiffness of materials. The shear modulus G defines the resistance to plastic deformation and B determines the resistance to fracture. Using the relations (4) and (5) the values of these parameters are calculated.

$$B = \frac{C_{11} + 2C_{12}}{3} n, \qquad (4)$$

$$G_H = \frac{G_R + G_V}{2}, \qquad (5)$$

where G_V and G_R are determined from the Eqs. (6) and (7), where V and R represent Voigt and Reuss bounds, respectively.

$$G_V = \frac{C_{11} - C_{12} \mp 3C_{44}}{5}, \qquad (6)$$

$$G_R = \frac{5(C_{11} - C_{12})C_{44}}{4C_{44} + 3(C_{11} - C_{12})}. \qquad (7)$$

The bulk module B of the compounds is listed in the Table II, we see that the values of B calculated with the elastic constants are in accordance with our results found previously. Our results indicate that Pd_2PrCl and Pd_2PrF are mechanically stable.

We have also calculated Young's modulus E which is a quantity that measures an object or substance's resistance to being deformed elastically (*i.e.*, non-permanently) when a stress is applied to it. The elastic modulus of an object is defined as the slope of its stress-strain curve in the elastic deformation region. A stiffer material will have a higher elastic modulus [33]. The Eq. (8) [34, 35] determines E according to G and B.

$$E = \frac{9BG}{3G + B}. \tag{8}$$

The value of the Young's modulus E is greater for Pd_2PrF as shown in Table II, so we can say that Pd_2PrF is the stiffer.

The Kleinman parameter ζ It describes the relative positions of cation and anion sub lattices under volume conserving strain distortions for which positions are not fixed by symmetry [36] and can be expressed as:

$$\zeta = \frac{C_{11} + 8C_{12}}{7C_{11} + 2C_{12}}. \tag{9}$$

It is current that the result of minimization of bond bending and bond stretching, respectively are $\zeta = 0$ and $\zeta = 1$. It is known that if the value of Kleinman parameter ζ is close to 0 the bond bending is dominated and when it closes to 1 the bond stretching is dominated. The calculated values of Kleinman parameter for our compounds are listed in Table II and the values are close to 1, thus in Pd_2PrCl and Pd_2PrF studied here the bond stretching will be dominated over bond bending.

The Lamé parameters (also called the Lamé coefficients, Lamé constants or Lamé moduli) are two material-dependent measures indicated by the first coefficient (λ) and second coefficient (μ) that arise in strain-stress relationships [37], this two coefficients are always positive for most of the materials and we can calculate them by the following relations (10)

$$\lambda = \frac{\nu E}{(1+\nu)(1-2\nu)}, \qquad \mu = \frac{E}{2(1+\nu)}. \tag{10}$$

Any material is isotropic when $\mu = (C_{11} - C_{12})/2$ [38], our compounds are satisfying this condition, hence they can be called as isotropic materials.

The degree of elastic anisotropy of a solid material is measured by the anisotropic ratio (A). theoretically, it defines how far a material is from being isotropic (if A = 1 the material is purely isotropic while it deviates from this value is called anisotropic material) and its mathematical definition is given by this following equation [39]:

$$A = \frac{2C_{44}}{C_{11} - C_{12}}. \tag{11}$$

As shown in Table. II, we observe that the values of A are not equal to unity, indicating the fact that our compounds are anisotropic.

Another important mechanical parameter is Cauchy pressure C_p, used to illustrate the bonding nature of compounds. If the pressure is positive the material is expected to be ductile, and in the case of a negative pressure it is brittle, the C_p is determined by the Eq. (12) [40].

$$C_p = C_{11} - C_{44}. \tag{12}$$

From the Table II, for our materials the value of Cp is positive, this shows that the compounds are ductile.

Pugh's ratio B/G [41] is also the factor which attributes to describe the brittle or ductile property of compounds, if B/G $>$ 1.75 the material is ductile, otherwise the material is brittle.

Our two materials are ductile because their B/G is larger than 1.75 which is equal to 3.11 and 2.47 for Pd_2PrCl and 2.69 and 3.10 for Pd_2PrF with GGA-PBE and GGA-PBE+U respectively.

The Poisson's ratio ν, It is defined as the ratio of transverse contraction strain to longitudinal extension strain in the direction of stretching force, is also another element which allows to defined the ductile/brittle character of a material, according to Frantsevich rule if the poisson's ratio is smaller than 1/3 the material will be brittle or else the material will be ductile [42], ν is determined by the following equation.

$$\nu = \frac{3B - 2G}{2(3B + G)}. \tag{13}$$

As shown in Table II, we observe that the values of ν are greater than 1/3 for Pd_2PrX with GGA-PBE and GGA-PBE+U, again confirming the above results.

TABLE III. Values of the energy gaps E_g (eV), the total, partial and interstitial magnetic moments per formula unit of the of Pd_2PrX (X=Cl,F) compounds by the GGA-PBE and GGA-PBE+U for the Hg_2CuTi-type structure.

		Methods	μ_{inters} (μB)	μ_{Pd1} (μB)	μ_{Pd2} (μB)	μ_{Pr} (μB)	$\mu_{Cl/F}$ (μB)	μ_{tot} (μB)	E_g (eV)	Band gap
Pd_2PrCl	Our work	GGA-PBE	0.210	-0.064	-0.065	1.954	-0.035	2.000	0.040	indirect (X-L)
		GGA-PBE+U	0.199	-0.088	-0.064	1.989	-0.036	2.000	0.060	indirect (X-L)
Pd_2PrF	Our work	GGA-PBE	0.177	-0.053	-0.054	1.931	-0.001	2.000	0.220	indirect (W-L)
		GGA-PBE+U	0.215	-0.037	-0.064	1.895	-0.009	2.000	0.250	indirect (W-L)

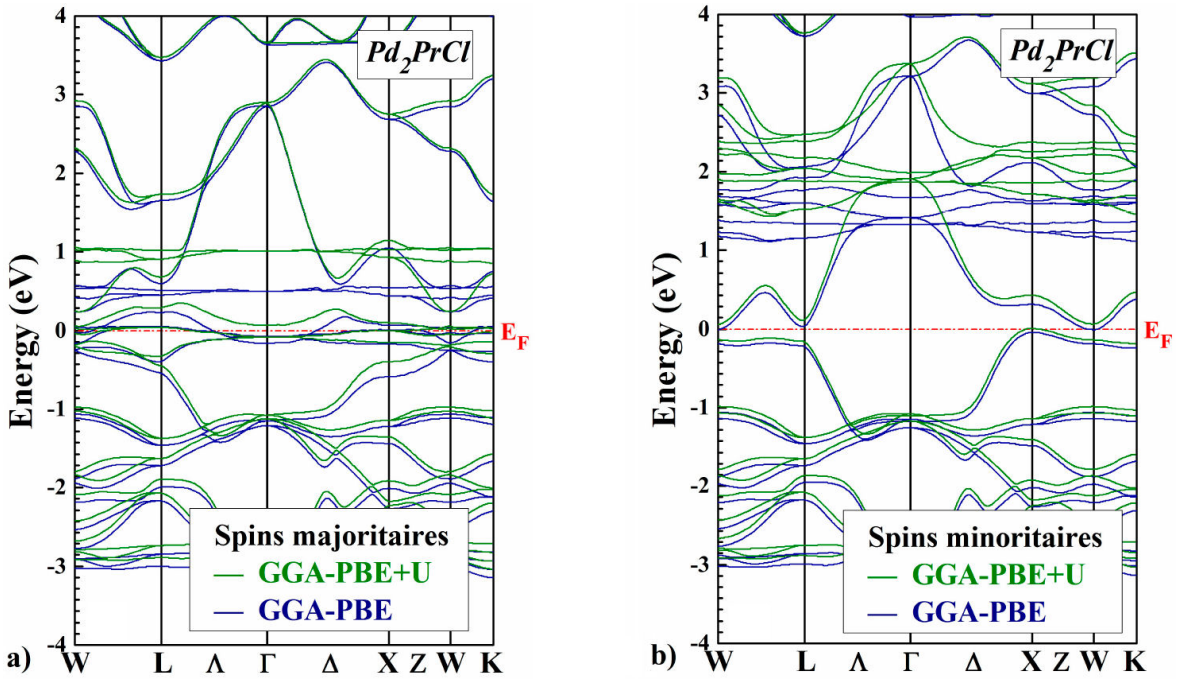

FIGURE 3. Comparison of GGA-PBE and GGA-PBE+U spin-polarized band structures a) spin up, and b) spin down of Pd_2PrCl for the Hg_2CuTi-type structure, calculated at the equilibrium lattice constant. The horizontal dashed line indicates the Fermi level.

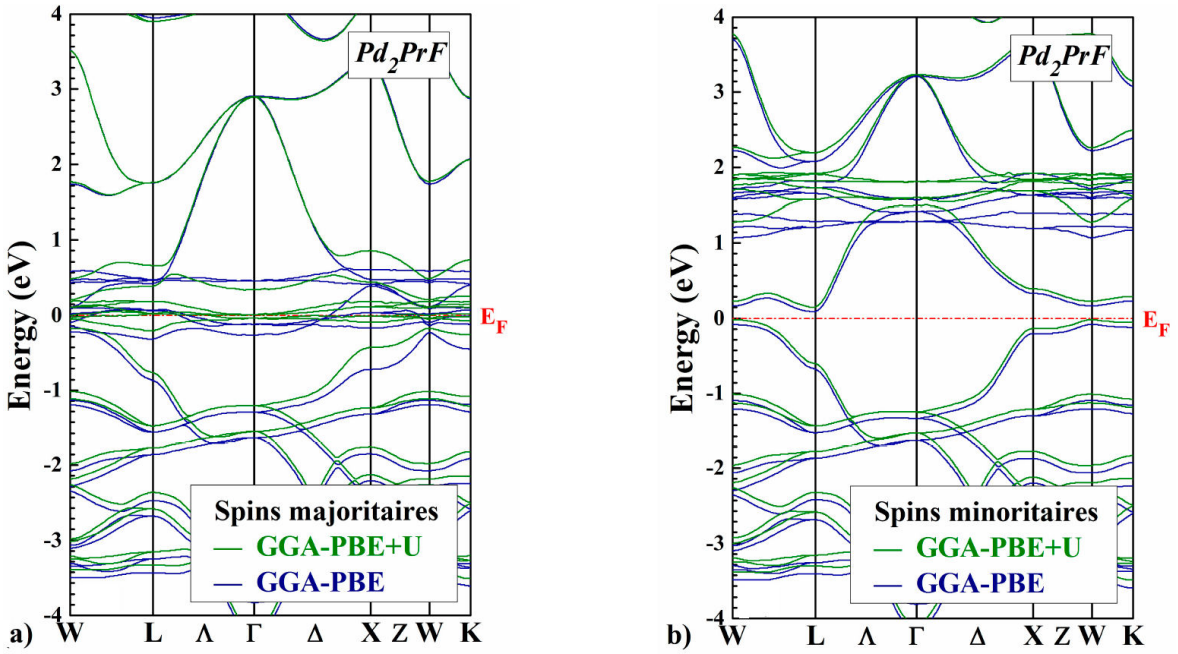

FIGURE 4. Comparison of GGA-PBE and GGA-PBE+U spin-polarized band structures a) spin up, and b) spin down of Pd_2PrF for the Hg_2CuTi-type structure, calculated at the equilibrium lattice constant. The horizontal dashed line indicates the Fermi level.

3.3. Electronic properties

The self-consistent scalar relativistic band structures for the Pd_2PrX (X=Cl ,F) along the various symmetry lines within the GGA-PBE and GGA-PBE+U scheme are given in Figs. 3 and 4, there is an overall topological resemblance for the two methods. The majority spin band is metallic, while the minority spin band shows a semiconducting gap around the Fermi level, where the values are shown in Table III.

The energy gap in the minority-spin band gap leads to 100% spin polarization at the Fermi level, resulting in the half-metallic behavior at equilibrium state.

The electron spin polarization (P) at the Fermi energy (E_F) of a material is defined by the following equation:

$$P = \frac{\rho\uparrow(E_F) - \rho\downarrow(E_F)}{\rho\uparrow(E_F) + \rho\downarrow(E_F)}, \quad (14)$$

where $\rho\uparrow$ and $\rho\downarrow$ are the spin up and spin down density of states at the Fermi level E_F [43].

The main difference which appears between the two approaches lies in the band gap of the spin-down channels of Pd_2PrX (X=Cl, F). More precisely, with GGA-PBE+U approach, we can see that the band gap is more significant than the previous two. For the two approaches, we observe that the minimum of conduction band is situated at the (W) point and the maximum of valence band is located at (Γ) point and (W) for Pd_2PrCl and Pd_2PrF respectively, this implies that Pd_2PrCl presents an indirect band gap equal to 0.06 eV and Pd_2PrF presents a indirect band gap equal to 0.25 eV with the GGA-PBE+U.

3.4. Magnetic properties

The calculated values of the total, local magnetic moments and the contribution of interstitial regions for Pd_2PrCl and Pd_2PrF with the GGA-PBE and GGA-PBE+U methods of the Hg_2CuTi-type are listed in the Table III, the magnetic moment is exactly 2 μB per unit cell.

The calculated total magnetic moment satisfies the rule of the Slater-Pauling behavior in the full-Heusler alloys [44]. M_{tot} is related to the total valence electrons (Z_{tot}) of alloys in this rule.

In order to obtain Slater-Pauling equations for HM Pd_2PrCl and Pd_2PrF compounds, the band structures of these alloys should be considered.

The majority spin bands are occupied with 17 electrons. Thus, the number of occupied minority states ($N\downarrow$) is calculated as:

$$N\downarrow = Z_{\text{tot}} - N\uparrow = Z_{\text{tot}} - 17, \quad (15)$$

where $N\downarrow$ is the number of occupied majority (spin-up) states. Therefore, M_{tot} is calculated as:

$$\begin{aligned} M_{\text{tot}} &= (N\uparrow - N\downarrow)\mu_B \\ &= (2N\uparrow - Z_{\text{tot}})\mu_B \\ &= (34 - Z_{\text{tot}})\mu_B \end{aligned} \quad (16)$$

Pd_2PrCl and Pd_2PrF compounds have 32 valence electrons (Z_{tot} = 32, 20 from the two Pd atoms, 5 from Pr and 7 from Cl (7 from F)), and M_{tot} according to Eq. (16) the M_{tot} is equal to 2 μB for our compounds which are in a good agreement with the results of Table III, as expected, all HM ferromagnets investigated exhibit an integer magnetic moment for the two methods. The magnetic moment is mainly localized on the Pr atom. Indeed, this atom contribute a large and positive magnetic moment, the magnetic moment on the Pd, Cl and F atoms are small.

3.5. Thermodynamic properties

The thermodynamic properties of Pd_2PrX (X=Cl, F) are determined by using the Debye model, implemented in the GIBBS code [28, 45], It treats the vibrations of the atomic lattice (heat) as phonons in a box, in contrast to the Einstein model, which treats the solid as many individual, noninteracting quantum harmonic oscillators. The Debye model correctly predicts the low temperature dependence of the heat capacity, which is proportional to T^3- the Debye T^3 law [46].

From the calculated energy-volume points, the quasiharmonic Debye model allows one to obtain all the thermodynamics quantities, in which the nonequilibrium Gibbs function $G^*(V,P,T)$ is expressed as follows [19]:

$$\begin{aligned} G^*(x,V;P,T) &= E_{sta}(x,V) + PV \\ &\quad + E^*_{Vib}(x,V;T) + F^*_{el}(x,V;T), \end{aligned} \quad (17)$$

which is a function of (V,P,T), where E_{sta} is the static energy and E^*_{Vib} is the vibrational Helmholtz free energy in nonequilibrium condition. The electronic free energy is described by F^*_{el}. The vibrational contribution in terms of Debye model is given as

$$F^*_{Vib} = \int_0^\infty \left(\frac{\omega}{2} + k_B T \ln\left[1 - e^{(\omega/k_B T)}\right] \right) g(\omega) d\omega, \quad (18)$$

where $g(\omega)$ is the phonon DOS (phDOS) and ω is the vibrational frequencies. Other thermodynamic properties such as entropy S, heat capacity C_v, thermal expansion coefficient (α) and Grüneisen parameter (γ) are calculated from the following relations:

$$S = S(V(P,T),T) = -\left(\frac{\partial F}{\partial T}\right)_V = \sum_j \left(-k_B \ln\left[1 - e^{\left(-\omega_j/k_B T\right)}\right] + \frac{\omega_j}{T} \frac{1}{e^{(\omega_j/k_B T)} - 1} \right), \quad (19)$$

$$C_V = C_\nu(V(P,T),T) = \left(\frac{\partial U}{\partial T}\right)_\nu = \sum_j C_{\nu,j} = \sum_j k_B \left(\frac{\omega_j}{k_B T}\right)^2 \frac{e^{\left(-\omega_j/k_B T\right)}}{(e^{(\omega_j/k_B T)} - 1)^2}, \quad (20)$$

$$\alpha = -\frac{1}{V}\left(\frac{\partial V}{\partial T}\right)_P = \frac{\gamma C_V}{V B_T}, \quad (21)$$

$$\gamma = -\frac{\partial \ln \Theta_D}{\partial \ln V}. \quad (22)$$

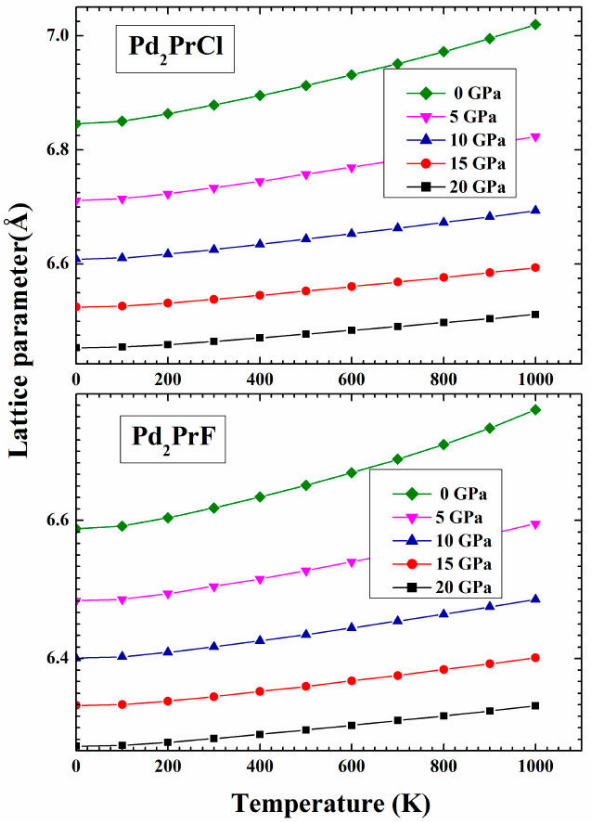

FIGURE 5. Lattice parameter versus temperature at different pressures for Pd_2PrCl and Pd_2PrF.

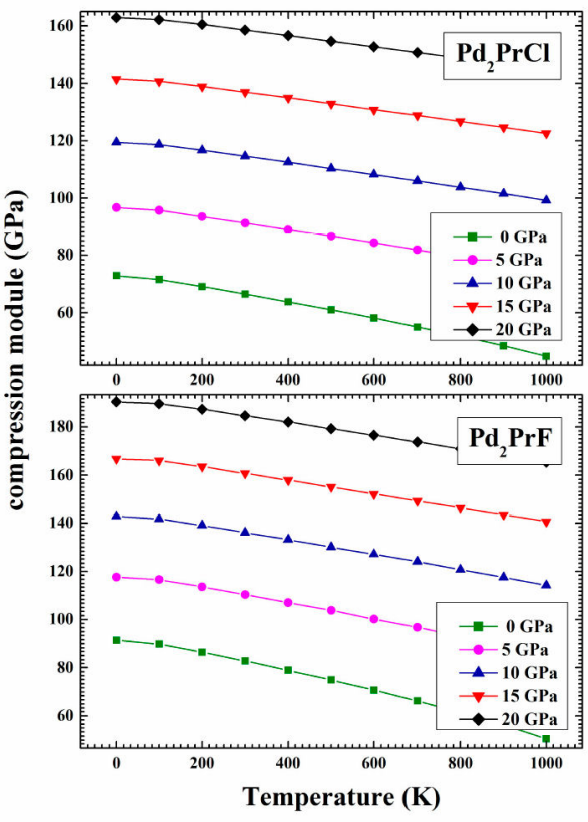

FIGURE 6. The compressibility module variation according to the temperature at different pressures for Pd_2PrCl and Pd_2PrF.

We employed the $E-V$ data (total energy E and volume V) of the primitive cell as data entered into the Gibbs program. These values E and V are determined in the previous part of the structural properties in the ground state $T = 0$ and $P = 0$ as part of the approximation (PBE-GGA) using the Wien2k code. These properties are determined in the temperature range from 0 K to 1000 K for Pd_2PrCl and Pd_2PrF.

The interest of the thermodynamic properties in material science motivated us to investigate the cell volume, bulk modulus and the specific heats C_ν at constant volume and pressure.

The variation of the lattice parameter as a function of the temperature at different pressures for our compounds Pd_2PrCl and Pd_2PrF respectively are represented in Fig. 5.

We observe that the parameter (a) increases with increasing temperature at a given pressure, but reduced with increasing pressure at a given temperature. The growth rate of the lattice parameter with reduced temperature and with increase pressure, temperature can cause expansion and pressure can suppress this effect.

The calculated values of lattice parameter for Pd_2PrCl and Pd_2PrF compounds respectively at $T = 300$ K and $P = 0$ GPa are equal to 6.87 and 6.61 Å.

The Bulk Modulus is a property that defines the resistance to change of volume when compressed [47], the compressibility module variation according to the temperature at different pressures for the two compounds Pd_2PrCl and Pd_2PrF is represented in Fig. 6, Unlike the lattice constant, the compressibility module B_0 increases with the increase of the pressure at a given temperature, and reduced with the increase of the temperature at a given pressure.

The calculated values of the compressibility module for Pd_2PrCl and Pd_2PrF respectively at $T = 300$ K and $P = 0$ GPa are equal to 66.07 GPa and 82.82 GPa.

The Debye temperature θ_D is the temperature of a crystal's highest normal mode of vibration, *i.e.*, the highest temperature that can be achieved due to a single normal vibration [48]. Figure 7 show the variation of the Debye temperature θ_D depending on the pressure and temperature for Pd_2PrCl and Pd_2PrF. We note that the debye temperature θ_D decreases with the increase of the temperature at a given pressure, and increases with increasing pressure to a given temperature and we can also note that θ_D is almost constant from 0 to 100 K and decreases when the temperature rises quadratically from $T > 100$ K, the Debye temperature values θ_D for Pd_2PrCl and Pd_2PrF respectively at $T = 300$ K and $P = 0$ GPa are equal to 271.64 and 304.49 K.

The Heat capacity C_V is an extensive property of matter, meaning that it is proportional to the size of the system. When expressing the same phenomenon as an intensive property, the heat capacity is divided by the amount of substance, mass, or volume, thus the quantity is independent of the size or extent of the sample [19].

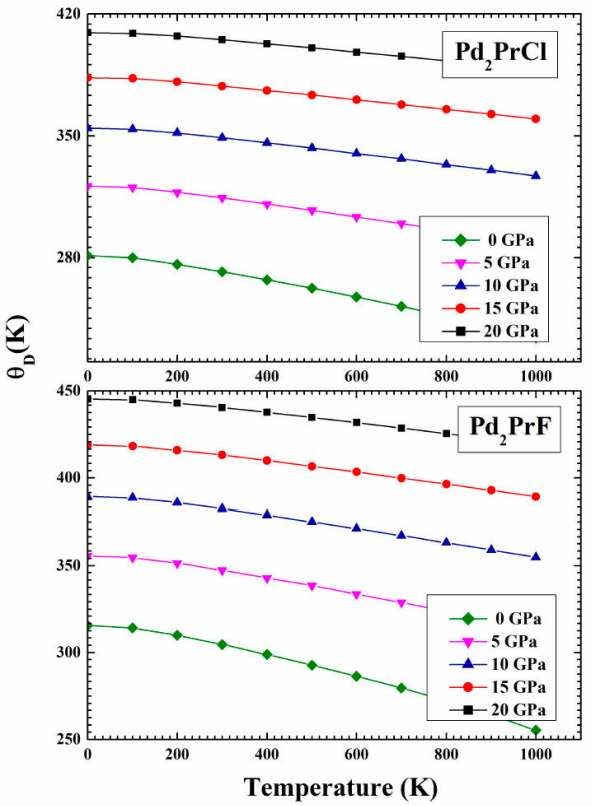

FIGURE 7. Debye temperature versus temperature at various pressures for Pd_2PrCl and Pd_2PrF.

Figure 8 represent the Variation of the heat capacity C_V versus temperature at some different pressures for Pd_2PrCl and Pd_2PrF, at Low temperature ($T < 500$, $T < 600$. k) for Pd_2PrCl and Pd_2PrF respectively, the heat capacity C_V is proportional to T^3.

For high temperatures C_V is quite close to the classic limit of Petit and Dulong [48]. Where C_ν approaches approximately 99.29 and 99.30 $JM^{-1}K^{-1}$ for Pd_2PrCl and Pd_2PrF respectively. The calculated values of heat capacity C_V at T = 300 K and P = 0 GPa are equal to 96.03 and 94.67 $JM^{-1}K^{-1}$ for Pd_2PrCl and Pd_2PrF respectively.

The Entropy of system S was introduced by Rudolf Clausius, he considered transfers of energy as heat and work between bodies of matter, taking temperature into account. Bodies of radiation are also covered by the same kind of reasoning [19]. The results of calculating the entropy according to the temperature at different pressures for Pd_2PrCl and Pd_2PrF are illustrated in Fig. 9.

We note that the entropy increases almost linearly with the increase temperature and decreases with each given pressure value. The calculated values of entropy S for Pd_2PrCl and Pd_2PrF respectively at $T = 300$ K and $P = 0$ GPa are equal to 146.50 and 134.81 $JM^{-1}K^{-1}$.

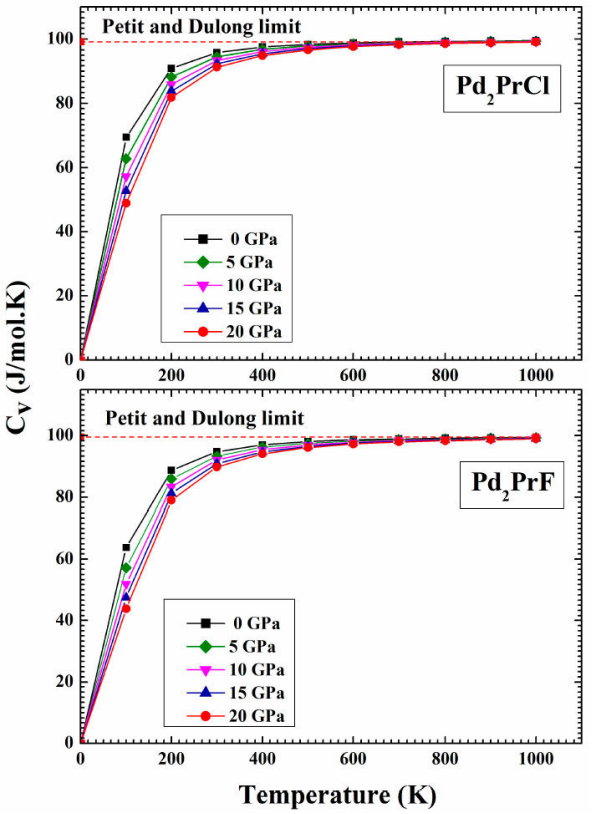

FIGURE 8. Heat capacity C_V versus temperature at different pressures for Pd_2PrCl and Pd_2PrF.

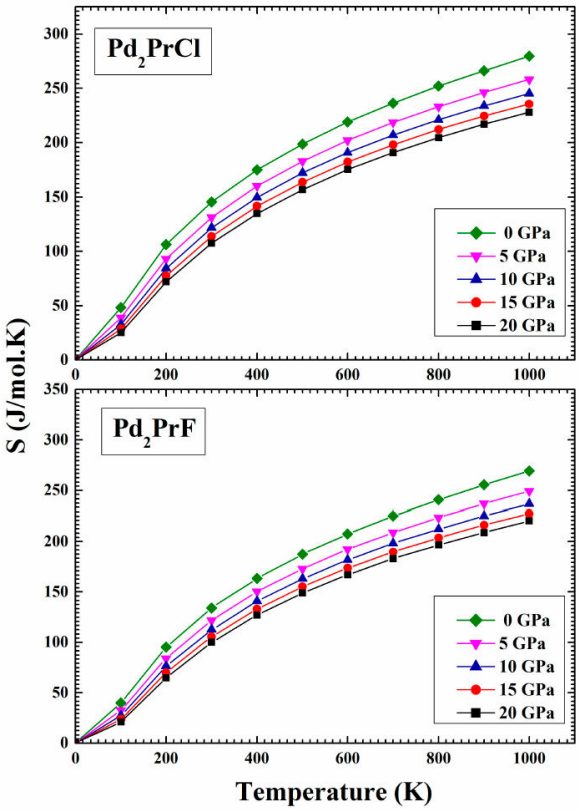

FIGURE 9. Entropy versus temperature at various pressures for Pd_2PrCl and Pd_2PrF.

4. Conclusion

In this work, the full-Heusler compounds Pd_2PrX (X = Cl, F) are explored. We have performed the calculations using WIEN2K package and PBE-GGA in the framework of Density Functional Theory (DFT). Elastic, mechanical, structural, electronic, magnetic and thermodynamic properties are derived and discussed.

Both the compounds are structurally stable in the ferromagnetic Hg_2CuTi-type structure. The negative values of formation energies E_f indicate these two alloys are easily fabricated experimentally and their formation processes are exothermic. The calculated values of cohesive energy E_c confirm that Hg_2CuTi structure in all compounds are more stable than Cu_2MnAl structure in FM state, and are negative, the absolute values are considerable.

Elastically, we found that the required mechanical stability criteria are satisfied and consequently our compounds are ductile and anisotropic material.

Electronic properties are analyzed with the band structures by GGA-PBE and GGA-PBE+U there is an overall topological resemblance for the two methods. Both the calculations have revealed that the majority spin band is metallic, while the minority spin band shows a small band gap around the Fermi level, which indicates that our compounds are half-metallic.

The calculated total magnetic moment of 2.00 μB per formula unit is very close to integer value and agree well with the Slater- Pauling rules ($M_{\text{tot}} = 34 - Z_{\text{tot}}$), where the partial spin moment of Pr which mainly contribute to the total magnetic moment.

Finally, we have conducted a detailed analysis of thermodynamic properties using the quasi-harmonic Debye-model implemented in the Gibbs2 code. So these full-Heusler compounds are candidate materials for future spintronic application.

Since there is no experimental or theoretical data to compare the obtained results. So our study is opened to experimental verifications because it is considered as the first theoretical predictions of the structural, elastic, mechanic, electronic, magnetic and thermodynamic properties for these compounds.

1. I. Žutić, J. Fabian, and S.D. Sarma, Spintronics: Fundamentals and applications. *Rev. Mod. Phys.*. **76** (2004) 323, https://doi.org/10.1103/RevModPhys.76.323
2. A. Hirohata, and K. Takanashi, Future perspectives for spintronic devices. *J. Phys. D: Appl. Phys* **47** (2014) 193001, http://iopscience.iop.org/0022-3727/47/19/193001
3. S. Benatmane, and B. Bouhafs. Investigation of new d0 half-metallic full-heusler alloys N2BaX (X= Rb, Cs, Ca and Sr) using first-principle calculations. *Computational Condensed Matter*, **19** (2019) e00371, 2019, https://doi.org/10.1016/j.cocom.2019.e00371
4. K. Kilian, and R. Victora. Electronic structure of Ni2MnIn for use in spin injection. *J. Appl. Phys.*, **87** (2000) 7064, https://doi.org/10.1063/1.372932
5. K.M. Wong. Study of the Electronic Structure of Individual Free-Standing Germanium Nanodots Using Spectroscopic Scanning Capacitance Microscopy. *Jpn. J. Appl. Phys.*, **48** (2009) 085002, https://iopscience.iop.org/article/10.1143/JJAP.48.085002
6. K. Wong, W. Chim, J. Huang, and L. Zhu. Scanning capacitance microscopy detection of charge trapping in free-standing germanium nanodots and the passivation of hole trap sites. *J. Appl. Phys.*, **103** (2008) 054505, https://doi.org/10.1063/1.2875776
7. K. Wong, W. Chim, and J. Yan. Physical mechanism of oxide interfacial traps, carrier mobility degradation and series resistance on contrast reversal in scanning-capacitance-microscopy dopant concentration extraction. *Appl. Phys. Lett.*, **87** (2005) 053504, https://doi.org/10.1063/1.2006979
8. K. Wong, and W. Chim. Deep-depletion physics-based analytical model for scanning capacitance microscopy carrier profile extraction. *Appl. Phys. Lett.*, **91** (2007) 013510, https://doi.org/10.1063/1.2753827
9. M. Johnscher *et al*., Rare-earth solid-state NMR spectroscopy of intermetallic compounds: The case of the 175Lu isotope. *Solid State Commun*, **52** (2016) 57, https://doi.org/10.1016/j.ssnmr.2019.05.003
10. S. Seidel, R.D. Hoffmann, R. Poettgen, and Z. Anorg, $LaRh_3Ga_2$ - Structure Determination from a Trilling. *Allg. Chem.*, **641** (2015) 1400, https://doi.org/10.1002/zaac.201500059
11. S. Seidel *et al*., Ternary rhombohedral Laves phases RE_2RH_3Ga (RE = Y, La-Nd, Sm, Gd-Er). *Z. Naturforsch. B*, **72** (2017) 289, https://doi.org/10.1515/znb-2016-0265
12. L. Heletta, S. Seidel, C. Benndorf, H. Eckert, and R. Poettgen, Gallium-containing Heusler phases $ScRh_2Ga$, $ScPd_2Ga$, $TmRh_2Ga$ and $LuRh_2Ga$-magnetic and solid state NMR-spectroscopic characterization. *Z. Naturforsch. B*, **72** (2017) 609, https://doi.org/10.1515/znb-2017-0084
13. C. Shekhar, S. Ouardi, A.K. Nayak, G.H. Fecher, W. Schnelle, and C. Felser, Ultrahigh mobility and nonsaturating magnetoresistance in Heusler topological insulators. *Phys. Rev. B*, **86** (2012) 155314, https://doi.org/10.1103/PhysRevB.86.155314
14. M. J. Winiarski, and K. Bilińska. High thermoelectric power factors of p-type half-Heusler alloys YNiSb, LuNiSb, YPdSb, and LuPdSb. *Intermetallic*, **108** (2019) 55, https://doi.org/10.1016/j.intermet.2019.02.009
15. A. Iyigör, M. Özduran, M. Ünsal, O. Örnek, and N. Arıkan, Ab-initio study of the structural, electronic, elastic and vibrational properties of HfX (X = Rh, Ru and Tc). *Philos. Mag. Lett.*, **97**

(2017) 110, https://doi.org/10.1080/09500839.2017.1290292

16. P. Blaha, K. Schwarz, P. Sorantin, and S. Trickey, Full-potential, linearized augmented plane wave programs for crystalline systems. *Comput. Phys. Commun.*, **59** (1990) 399, https://doi.org/10.1016/0010-4655(90)90187-6

17. P. Hohenberg, and W. Kohn, Inhomogeneous Electron Gas. *Phys. Rev.*, **136** (1964) B864, https://doi.org/10.1103/PhysRev.136.B864

18. K. Schwarz, P. Blaha, and G. Madsen, Electronic structure calculations of solids using the WIEN2k package for material sciences. Comput. Phys. Commun., **147** (2002) 71, https://doi.org/10.1016/S0010-4655(02)00206-0

19. M. Blanco, E. Francisco, and V. Luana, GIBBS: isothermal-isobaric thermodynamics of solids from energy curves using a quasi-harmonic Debye model. *Comput. Phys. Commun.*, **158** (2004) 57, https://doi.org/10.1016/j.comphy.2003.12.001

20. Z. Wen, Y. Zhao, H. Hou, B. Wang, and P. Han, The mechanical and thermodynamic properties of Heusler compounds Ni2XAl (X = Sc, Ti, V) under pressure and temperature: A first-principles study. *Mater. Des.*, **114** (2017) 398, https://doi.org/10.1016/j.matdes.2016.11.005

21. D. Rai, A. Shankar, M. Ghimire, and R. Thapa, Electronic and magnetic properties of a full-Heusler alloy Co2CrGe: a first-principles study. *J. Theor. Appl. Phys*, **7** (2013) 3, https://doi.org/10.1186/2251-7235-7-3

22. T. Song, X.W. Sun, J.H. Tian, X.P. Wei, G.X. Wan, and Q. Ma, The effect of pressure on the structural, electronic, magnetic, and thermodynamic properties of the Mn2RuGe inverse Heusler alloy. *J. Magn. Magn. Mater*, **428** (2017) 287, https://doi.org/10.1016/j.jmmm.2016.12.076

23. A. Bentouaf, F.H. Hassan, A.H. Reshak, and B. Aïssa, First-Principles Study on the Structural, Electronic, Magnetic and Thermodynamic Properties of Full Heusler Alloys Co_2VZ (Z = Al, Ga). *J. Magn. Magn. Mater*, **46** (2017) 130, https://doi.org/10.1007/s11664-016-4859-9

24. L. Hao, R. Khenata, X. Wang, and T. Yang, Ab Initio Study of the Structural, Electronic, Magnetic, Mechanical and Thermodynamic Properties of Full-Heusler Mn_2CoGa. *J. Electron. Mater.*, **48** (2019) 6222, https://doi.org/10.1007/s11664-019-07417-x

25. X. Wang, Z. Cheng, and G. Liu, Largest Magnetic Moments in the Half-Heusler Alloys XCrZ (X = Li, K, Rb, Cs; Z = S, Se, Te): A First-Principles Study. *Materials*, **10** (2017) 1078, https://doi.org/10.3390/ma10091078

26. J.P. Perdew, K. Burke, and M. Ernzerhof, Generalized Gradient Approximation Made Simple. *Phys. Rev. Lett.*, **77** (1996) 3865, https://doi.org/10.1103/PhysRevLett.77.3865

27. V.I. Anisimov, J. Zaanen, and O.K. Andersen, Band theory and Mott insulators: Hubbard U instead of Stoner *I. Phys. Rev. B*, **44** (1991) 943, https://doi.org/10.1103/PhysRevB.44.943

28. H.J. Monkhorst, and J.D. Pack, Special points for Brillouin-zone integrations. Phys. Rev. B, **13** (1976) 5188, https://doi.org/10.1103/PhysRevB.13.5188

29. F.D. Murnaghan, The Compressibility of Media under Extreme Pressures. *Proc. Natl. Acad. Sci. USA*, **30** (1944) 244, https://doi.org/10.1073/pnas.30.9.24

30. P. Vinet, J.H. Rose, J. Ferrante, and J.R. Smith, Universal features of the equation of state of solids. *J. Phys. Condens. Matter*, **1** (1989) 1941, https://doi.org/10.1088/0953-8984/1/11/002

31. M. Born, and K. Huang, Dynamical theory of crystal lattices, *Clarendon press*, **1954**, https://doi.org/10.1107/S0365110X56002370

32. M. Born, On the stability of crystal lattices. *J. Chem. Phys*, **7** (1939) 591, https://doi.org/10.1017/S0305004100017138

33. H.B. Pedersen, and J.L. Knudsen, Direct determination of the non-linear connection between tension and transverse amplitude for a vibrating string. *Eur. J. Phys.*, **38** (2017) 045003, https://doi.org/10.1088/1361-6404/aa68fc

34. Z.E. Wu Z. J. H. Xiang, X. Hao, X. Liu, and J. Meng, Crystal structures and elastic properties of superhard IrN2 and IrN3 from first principles. *Phys. Rev. B*, **76** (2007) 054115, https://doi.org/10.1103/PhysRevB.76.054115

35. F. Peng, L. Han, H. Fu, and X. Cheng, First-principles calculations on elasticity and the thermodynamic properties of TaC under pressure. *Phys. Status Solidi B*, **246** (2009) 1590, https://doi.org/10.1002/pssb.200945014

36. R. Majumder, and M.M. Hossain, First-principles study of structural, electronic, elastic, thermodynamic and optical properties of topological superconductor LuPtBi. *Comput. Condens. Matter*, **21** (2019) e00402, https://doi.org/10.1016/j.cocom.2019.e00402

37. C. Liu, J. Yu, B. Zhang, and X. Zhang, Elastic wave attenuation in a functionally graded viscoelastic couple stress plate, sandwiched between two elastic half-spaces. *Appl. Math. Model*, **75** (2019) 52, https://doi.org/10.1016/j.apm.2022.04.013

38. S. Ahmad, M. Shafiq, R. Ahmad, S. Jalali-Asadabadi, and I. Ahmad, Strongly correlated intermetallic rare-earth monoaurides (Ln-Au): Ab-initio study. *J. Rare Earths*, **36** (2018) 1106, https://doi.org/10.1016/j.jre.2018.03.018

39. C. Zener, Interaction between the d-Shells in the Transition Metals. II. Ferromagnetic. *Phys. Rev*, **82** (1951) 403, https://doi.org/10.1103/PhysRev.82.403

40. V. Kanchana, G. Vaitheeswaran, Y. Ma, Y. Xie, A. Svane, and O. Eriksson, Density functional study of elastic and vibrational properties of the Heusler-type alloys Fe2VAl and Fe2VGa. *Phys. Rev. B*, **80** (2009) 125108, https://doi.org/10.1103/PhysRevB.80.125108

41. X. Wang, Z. Cheng, J. Wang, and G. Liu, A full spectrum of spintronic properties demonstrated by a C1b-type Heusler compound Mn2Sn subjected to strain engineering. *J. Mater. Chem. C*, **4** (2016) 8535, https://doi.org/10.1039/C6TC02526A

42. P. Mott, J. Dorgan, and C. Roland, The bulk modulus and Poisson's ratio of "incompressible" materials. *J. Sound Vib.*, **312** (2008) 572, https://doi.org/10.1016/j.jsv.2008.01.026

43. R. Soulen *et al*., Measuring the Spin Polarization of a Metal with a Superconducting Point Contact. *Science*, **282** (1998) 85, 10.1126/science.282.5386.85

44. K. Özdogan, E. Sasıoglu, and I. Galanakis, Slater-Pauling behavior in LiMgPdSn-type multifunctional quaternary Heusler materials: Half-metallicity, spin-gapless and magnetic semiconductors. *J. Appl. Phys*, **113** (2013) 193903, https://doi.org/10.1063/1.4805063

45. R.G. Pearson, Maximum Chemical and Physical Hardness. *J. Chem. Educ.*, **76** (1999) 267, https://doi.org/10.1021/ed076p267

46. P. Debye. Rationalizing phonon dispersion for lattice thermal conductivity of solids. *Ann. Phys*., **344** (1912) 789, https://doi.org/10.1093/nsr/nwy097

47. M. Flórez, J. Recio, E. Francisco, M. Blanco, and A.M. Pendás. First-principles study of the rocksalt-cesium chloride relative phase stability in alkali halides. *Phys. Rev. B*, **66** (2002) 144112, https://doi.org/10.1103/PhysRevB.66.144112

48. A. Petit, and Dulong, Can quantum-mechanical description of physical reality be considered complete?. *Ann. Chim. Phys.*, **10** (1819) 395, https://doi.org/10.1103/PhysRev.47.777